

# The LINC-NIRVANA fringe and flexure tracker: an update of the opto-mechanical system

Jens Zuther<sup>a</sup>, Andreas Eckart<sup>a</sup>, Thomas Bertram<sup>b</sup>, Matthew Horrobin<sup>a</sup>, Bettina Lindhorst<sup>a</sup>, Uwe Lindhorst<sup>a</sup>, Lydia Moser<sup>a</sup>, Steffen Rost<sup>a</sup>, Christian Straubmeier<sup>a</sup>, Evangelia Tremou<sup>a</sup> and Imke Wank<sup>a</sup>

<sup>a</sup>I. Physikalisches Institut, Universität zu Köln, Zùlpicher Str. 77, D-50937 Köln, Germany;  
<sup>b</sup>Max-Planck Institut für Astronomie, Königsstuhl 17, D-69117 Heidelberg, Germany

## ABSTRACT

LINC-NIRVANA (LN) is a German/Italian interferometric beam combiner camera for the Large Binocular Telescope. Due to homothetic imaging, LN will make use of an exceptionally large field-of-view. As part of LN, the Fringe-and-Flexure-Tracker system (FFTS) will provide real-time, closed-loop measurement and correction of piston and flexure signals induced by the atmosphere and inside the telescope-instrument system. Such compensation is essential for achieving coherent light combination over substantial time intervals ( $\sim 10$ min.). The FFTS is composed of a dedicated near-infrared detector, which can be positioned by three linear stages within the curved focal plane of LN. The system is divided into a cryogenic (detector) and ambient (linear stages) temperature environment, which are isolated from each other by a moving baffle. We give an overview of the current design and implementation stage of the FFTS opto-mechanical and electronic components. We present recent important updates of the system, including the development of separated channels for the tracking of piston and flexure. Furthermore, the inclusion of dispersive elements will allow for the correction of atmospheric differential refraction, as well as the induction of artificial dispersion to better exploit the observational-conditions parameter space (air mass, brightness).

**Keywords:** LBT, LINC-NIRVANA, fringe tracking, flexure tracking

## 1. INTRODUCTION

LINC-NIRVANA (LN) is a near-infrared interferometric beam combiner camera<sup>1</sup> built by a German/Italian consortium for the Large Binocular Telescope (LBT). To guarantee coherent light combination over long integration times (up to 10min.), a fringe and flexure tracking system (FFTS)<sup>2</sup> is required. By tracking a bright point-source reference (PSF) within the isopiston patch, optical path differences (OPD), introduced by the atmosphere and by the telescope-instrument system, can be assessed<sup>3</sup> and feed back into a real-time control loop<sup>4</sup>, controlling a movable mirror. The piezo-driven mirror can modify the optical path length of the light paths of both mirrors of the LBT, thereby eliminating OPD with respect to the science detector. The PSF will be sampled by the FFTS detector<sup>5</sup> at a rate of 50-200Hz. The required residual OPD is supposed to be less than  $\lambda/10$ . Flexure within the telescope-instrument system will cause misalignment of the two optical axes of the two optical paths. Analysis of the 2-D intensity distribution of the fringe-tracking PSF can be used to estimate the misalignment of the two beams. The time scale for flexure detection is significantly less ( $\sim 1$ Hz)<sup>6</sup> than for OPD variation, which allows for integration over several short fringe exposures to gain S/N with respect to the Airy distributions of the two single-eye telescopes. Residual flexure is required to be on the sub-pixel scale (1 pixel corresp. to  $18.5\mu\text{m}$ , considerably less than 1 Airy radius). In contrast to the fringe signal, the flexure signal has to be feed back to the telescope and adaptive optics control systems.

---

Further author information: (Send correspondence to J. Zuther)

J. Zuther: E-mail: zuther@ph1.uni-koeln.de, Telephone: ++49 (0)221 470 3495

## 2. SEPARATING FRINGE AND FLEXURE CHANNELS

Until recently, it was foreseen to carry out fringe and flexure tracking on the same interferometric image on the FFTS detector<sup>2</sup>. However, it is advantageous<sup>6</sup> to separate fringe and flexure channels on the FFTS detector (Fig. 1). In the following, flexure tracking should rather be called image motion tracking, since there are several causes for image motion in the focal plane, flexure being one of them:

1. Atmospheric tip/tilt.
2. Flexure in the optical path that is common to the mid-high wave-front system (MHWS;<sup>7</sup> adaptive optics system senses at visible wavelengths) and NIR channel, i.e. telescope-to-instrument interface.
3. Flexure in the non-common optical path (e.g., warm dichroic, K-mirror, patrol camera mirror, MHWS sensor, cryostat with cold optics).
4. Atmospheric differential refraction (ADR).
5. Misalignment of K-mirror axis, science detector rotation axis, and FFTS axis, as well as, flexure of the FFTS.

In the old concept the MHWS only deals with fast, i.e. atmospheric, tip/tilts. Image motion tracking and slow tip/tilts are left for being handled as part of the fringe tracking of the interferometric PSF. In the revised concept, the MHWS takes care of all tip/tilts it recognizes. All effects in 1. and 2. are taken care of by the MHWS. The image motion channel of the FFTS is left to deal with flexure in the non-common path (3.) and ADR (4.). Effects described in 5. can be calibrated (see, e.g., Ref. 8 for a discussion of flexure of the FFTS). A simplified version of the revised control scheme to remove non-common path flexure is presented in Fig. 2. Two scenarios, which are currently evaluated, are possible: (i) direct control of the warm dichroic of the AO system or (ii) passing tip/tilt information to the wave-front data handling system (WDHS). Details about the image analysis and the control scheme can be found in Refs. 3 and 4.

The major requirements for *slow* image motion tracking, which will also determine the system modifications described in the next Section, are:

1.  $< 1$  pixel rms deviation of the images of the single-eye PSFs from the nominal position on the science detector,
2. accessibility of full FOV ( $60'' \times 90''$  on sky),
3.  $\pm 1''$  range for initial setup (recover from a blind pointing),
4. 1 Hz sampling frequency, 0.1Hz control bandwidth.

In order to measure image motion (e.g., by fitting the photo center) and attribute it to the single-eye optical paths individually, a clear separation of the beams is profitable. This can be achieved by defocusing (Fig. 3; cf., Sec. 3 for a realization).

### 2.1 In search for an optimized channel separation

At this point, we assume a Strehl 1 situation. More realistic ones will be investigated in a next step<sup>3</sup>. The question is at what combination of defocus, fraction of light split into the image motion tracking channel (related to S/N), and bandwidth can we expect a performance that fulfills the requirements.

Figure 3 shows the effect of defocus at  $2.2\mu\text{m}$  of the interferometric PSF. For example, at a defocus of 20mm, the two single-eye Airys are separated by almost one Airy radius. At smaller defocus, intermediate fringes make it more difficult to unambiguously separate the two PSFs and determine their photo centers. The effect of defocus is more pronounced at shorter wavelengths. Above 20mm defocus, the two Airys are well separated at all FFTS wavelengths ( $1.2 - 2.2\mu\text{m}$ ).

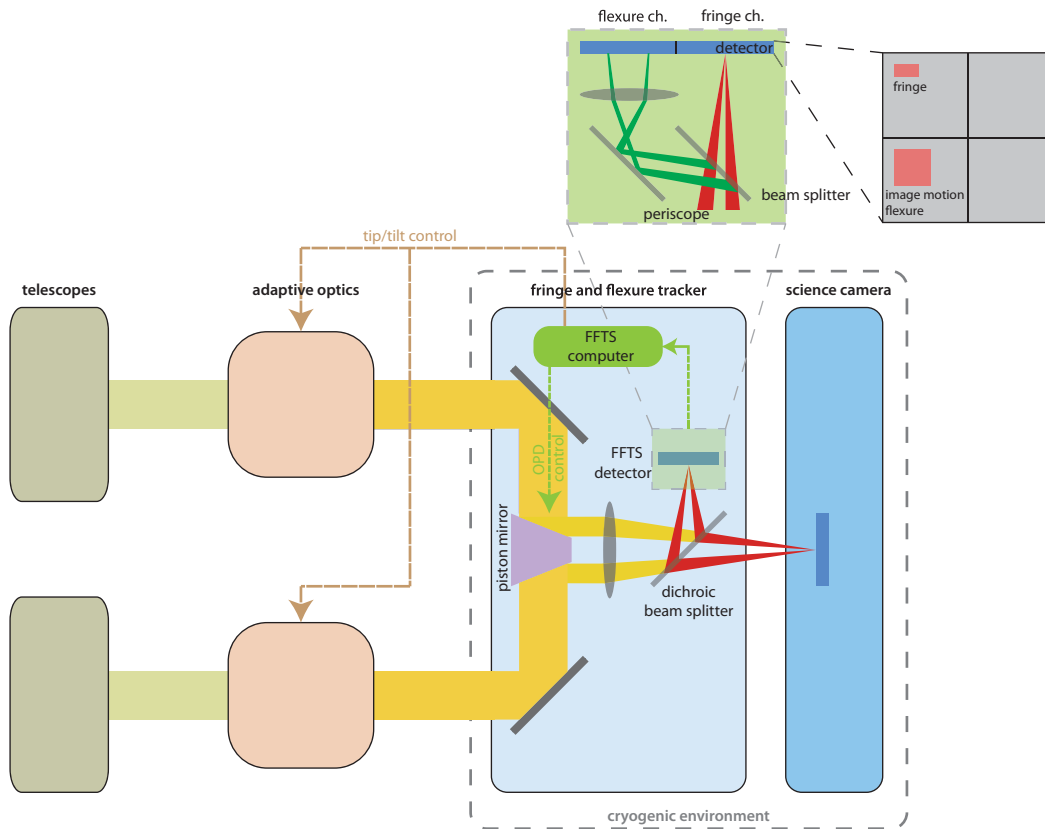


Figure 1. Schematics of the revised fringe and flexure tracker system (cf., Fig. 2 in Ref. 6). Separation of fringe and image motion tracking is achieved with a periscope setup, perpendicular to the LBT baseline (zoom in, left part). Readout windows are red (zoom in, right part: e.g.,  $16 \times 32$  pixel for fringe tracking and  $64 \times 64$  pixel for image motion tracking). In order to optimize read out speed, the windows, especially the fringe tracking channel, are located in a corner of the respective quadrant (depending on the orientation of the detector with respect to the baseline).

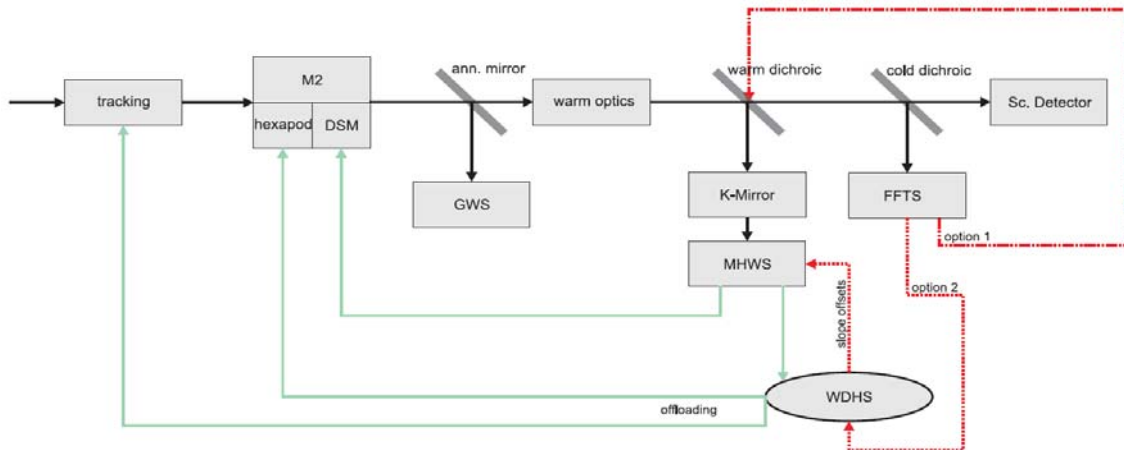


Figure 2. Simplified tip/tilt control scheme for LINC-NIRVANA. Based on the new flexure (slow image motion) channel, tip/tilt information can either be provided directly to the warm dichroic of adaptive optics system or to the wave-front data handling system (WDHS). Compare Ref. 4.

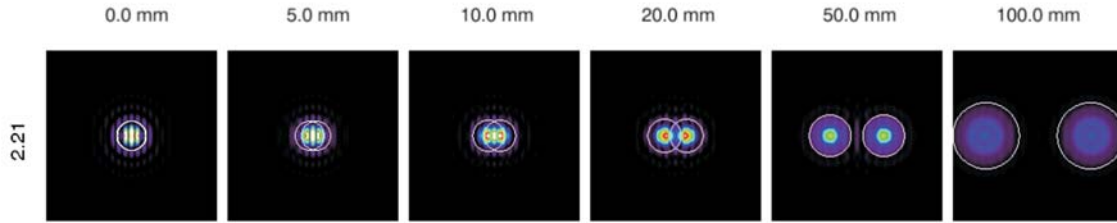


Figure 3. 2-D intensity distribution of LBT PSF as function of defocus at  $2.2\mu\text{m}$ . White circles indicate the region containing 84% of the single eye PSF flux. At a common defocus of about 20mm, the beams are well separated at all core FFTS wavelengths, which is necessary for image motion tracking (intermediate interference, shift of centroid position) .

We carried out simulations of the lateral sensitivity at the presence of noise (adding Gaussian noise according to the desired S/N and a random sub-pixel displacement). Figure 4 shows the dependence of the centroid fitting error as a function of defocus and S/N. The plots represent the case, in which the position of the PSF is uncertain by  $\pm 0.3$  pixel. The fitting error corresponds to the sensitivity, with which slow image motion can be detected. It should be smaller than the requirement on the maximum acceptable rms image motion of 1 pixel (see above). An additional demagnification (by a lens in the image motion tracking channel) could reduce the spot sizes, concentrating light and simultaneously increase the S/N. However, it also reduces the lateral sensitivity. The four panels in Fig. 4 show the dependence of the centroid fitting error for several demagnifications (factor of 1, 2, 3, and 3.5). As is evident from the simulation, the best performance at low S/N ( $\sim 5$ ) is achieved with a demagnification of a factor of 3 and a defocus of about 25mm. A lateral sensitivity of 0.3 pixel was chosen as a baseline.

Table 1. S/N of image motion tracking channel as a function of the fraction,  $\eta$ , of light split into the image motion tracking channel and the frame rate in the image motion tracking channel ( $R_{\text{IM}}$ ).

$\lambda_{\text{science}}$	$\eta$ (& $\Delta\text{mag}$ )	$R_{\text{IM}} =$	0.2Hz	0.4Hz	0.6Hz	0.8Hz	1.0 Hz
$K$	0.05 (0.06)		5.8	3.1	2.2	1.7	1.0
$K$	0.1 (0.11)		10.5	6.0	4.2	3.3	2.7
$J$	0.1 (0.11)		18.0	11.0	8.0	6.0	5.0

A fraction of light has to be split into the image motion tracking channel, thereby reducing the sensitivity of the fringe tracking channel. A 5% (10%) fraction in the image motion tracking channel corresponds to a loss of sensitivity in terms of limiting magnitudes of about 0.06mag (0.11mag) for the fringe tracking channel. Table 1 shows the S/N in the image motion tracking channel dependent on the amount of light split into the channel and the frame rate of the image motion tracking channel. The table has been computed, assuming that in each band the minimum required S/N is achieved in the fringe channel at 100Hz frame rate. To achieve the required  $S/N \sim 5$  for sub-pixel centroid fitting, for 10% fraction in the image motion tracking channel frame rate of the order of 0.5Hz are required. To improve on this, a higher fraction of the incoming light can be dedicated to the image motion tracking channel. However, since in the new scheme only slow image motion is tracked by the FFTS, such small frame rates might be sufficient. The bandwidth for slow image motion is currently under investigation.

### 3. IMPLICATIONS FOR THE OPTO-MECHANICAL DESIGN

The fringe and image motion tracking channels will be separated onto different quadrants of the FFTS detector. The image motion tracking channel will be deflected perpendicular to the interferometer baseline by a periscope (Fig. 5(d)).<sup>6</sup> An important side effect is the occurrence of beam walk in the image motion channel, because of changing field angles ( $\sim 9.8^\circ$  in each direction) from the two single-eye telescopes within the  $60'' \times 90''$  FOV. For optimal channel separation, i.e. a defocus of 25mm, the beam walk amounts to 230 pixel (270 pixel when

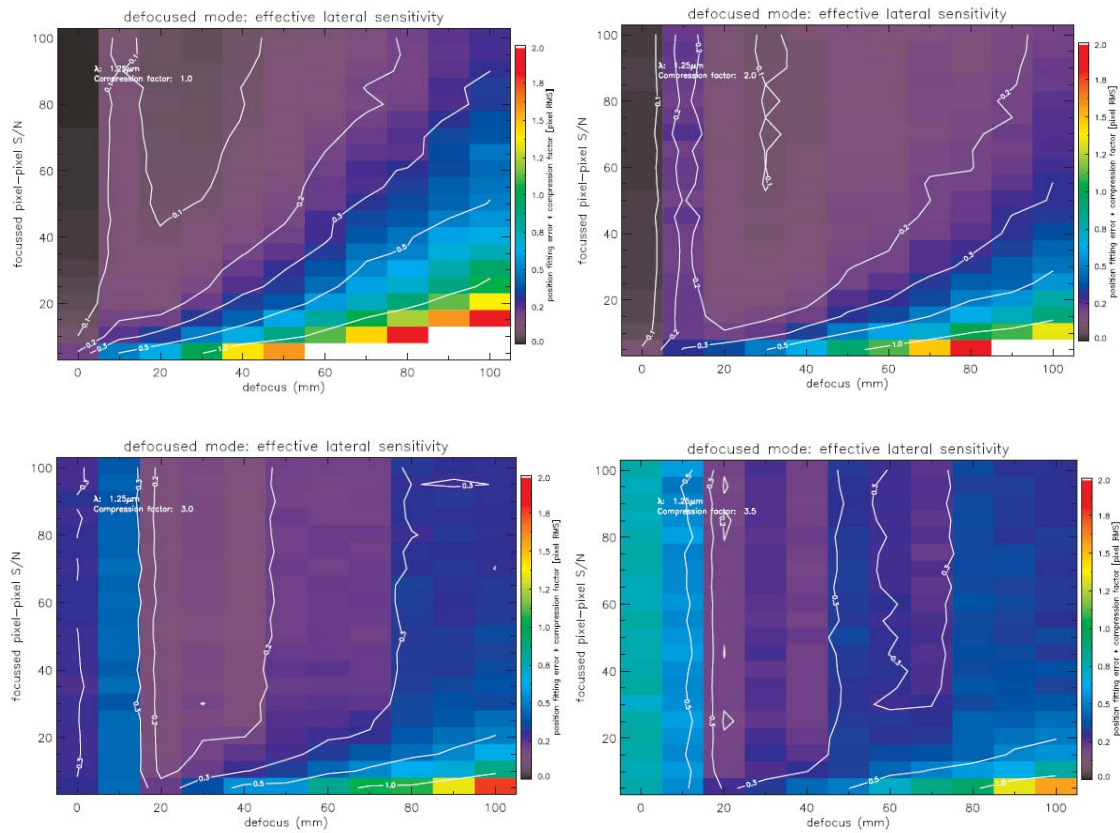


Figure 4. Effective lateral sensitivity for different S/N conditions, different values of compression factors (from left to right and top to bottom: 1, 2, 3, 3.5) at  $\lambda = 1.25\mu\text{m}$ . The S/N values shown here refer to pixel-to-pixel S/N of a focused single-eye PSF. The effective lateral sensitivity is defined as the position fitting rms [pixel] times the compression factor. The leftmost region of each plot should be omitted, since the signal is dominated by the interferometric overlap of the two Airys. Note that for a compression of 3 and a defocus of about 25mm, an optimal configuration is achieved.

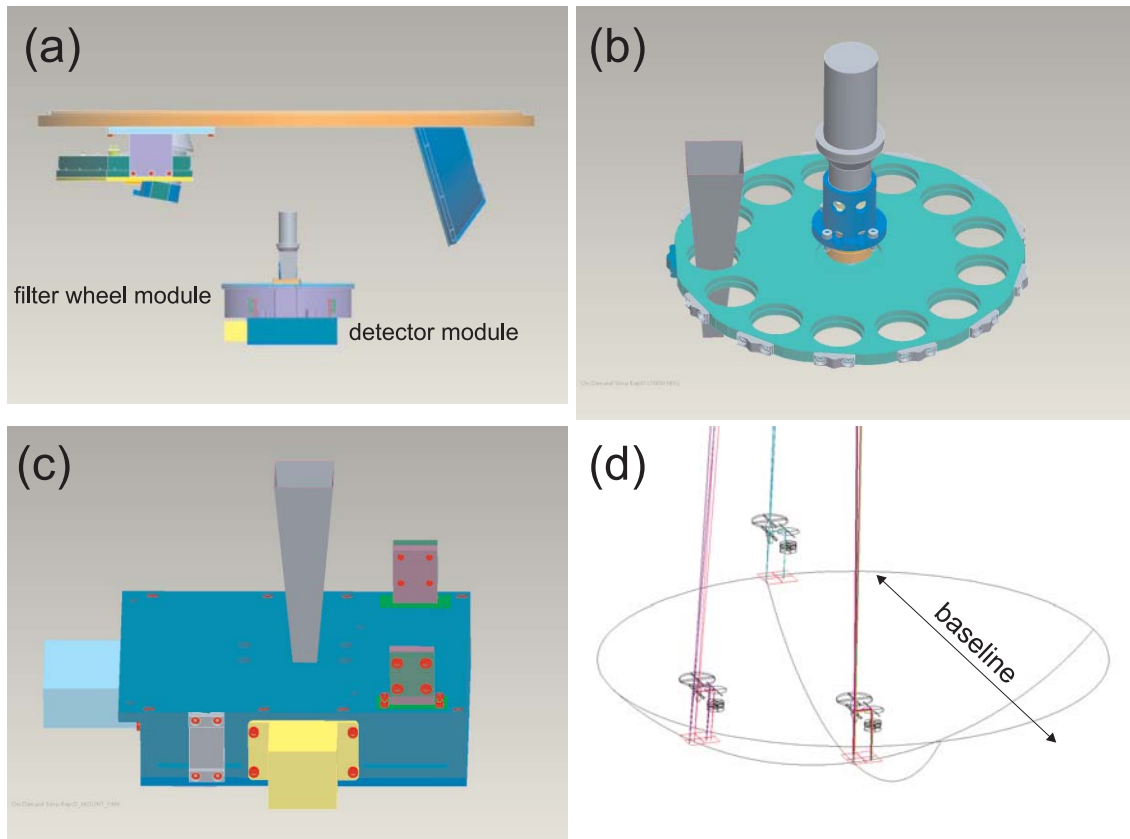


Figure 5. Opto-mechanical design. (a) The FFTS detector head, consisting of the detector module (detector, fanout board, interface to the pin connecting to the ambient temperature x-y-z linear stages, periscope) and the filter wheel module (filter wheel, wedges, motor), in relation to other cold optics (left: dichroic; right: science filter wheel). See Fig. 1 in Ref. 6 for an overall system layout. (b) Filter wheel and motor. The grey cone shape represents the envelope of the two telescope beams assuming maximum field angles. (c) Detector module showing the beam envelope (grey), cooling connectors (green-violet; one for the detector, the other for amplifiers on the read out board), and cable connectors (yellow, light blue). The latter will allow for easy disassembly in case of maintenance. (d) optical layout of the periscope, shown in three positions within the focal plane (field-of-view) of the FFTS.

including the extend of the defocused PSF). Regarding the operational requirement of 10 min. closed-loop observing, the beam walk range reduces considerably. Then, being a function of the zenith distance, a typical window size is about half the full beam walk. Implementing a demagnification of a factor 3 further reduces the beam walk by the same factor. The resulting window sizes nicely fit within each quadrant of the  $1024 \times 1024$  Hawaii-I detector. The window size also determines the frame rate at which the information can be read from the detector.

The current design of the detector head is presented in Fig. 5. The detector head consists of two modules, the detector module and the filter wheel module. The former contains the detector, the fanout board, the interface to the pin connecting the detector head through the baffle to the detector positioning unit (3 linear stages; cf., Fig. 3 in Ref. 9) and the periscope. The latter consists of the filter wheel plus motor and wedges. It will be mounted on top of the detector housing and can be assembled and disassembled in a modular way. Major updates concern the periscope, the filter wheel, as well as the layout of the detector housing.

The periscope will be attached to the detector module, since a constant alignment of the periscope and the detector has to be guaranteed. Goal is a compact design, however important size constraints are given by the beam envelope (sketched by the grey cone-like structure in Fig. 5(b, c)) and the distance to other cryogenic components like the science filter wheel and the dichroic (Fig. 5(a)). Extrafocal channel separation and demagnification is required for the beam walk to happen in the image motion tracking path. The beam splitter and the folding mirror are inclined by  $45^\circ$  and oriented such that the image motion tracking beam, including beam walk, reached the FFTS detector in the upper corner of the second quadrant (Fig. 5(d)). Currently, we split a 10% fraction of the incoming light into the image motion tracking channel. A lens will be used to image the defocused beams with a demagnification of factor 3 onto the FFTS detector. We are currently experimenting with a single lens solution with the goal to assemble the periscope with off-the-shelf optical components. The clear aperture diameters of the optical components will be given by the beam diameter and beam walk and amounts to 6mm at the position of the filters.

The filter wheel has been resized. Starting with the original filter set (J, H, K, J+H, H+K, narrow band, open, and blank) we added another set of filters with two wedges attached to each of its filters (J, H, K, J+H, H+K). The wedges are used to compensate atmospheric differential refraction (ADR)<sup>10</sup> or to introduce artificial dispersion. Figure 6 shows the effects of ADR as an elongation of the PSF especially at short wavelengths (J) and in very broad band filters (J+H and H+K). ADR compensation is important to maintain the sensitivity and not to spectrally distribute the PSF light during observations at low airmass (e.g., the Galactic Center<sup>11</sup>). On the other hand, dispersed fringes hold information on the OPD in terms of the pitch with respect to the nominal 0th order fringe orientation,<sup>3</sup> though such a mode is of main interest for bright sources only. Since ADR becomes significant for zenith distances above  $40^\circ$ , we are currently implementing two wedges per additional filter, corresponding to  $40^\circ$  and  $60^\circ$ . The wedges will be attached at the bottom of the filter wheel. The clear aperture of each filter is large enough ( $r \sim 10.7\text{mm}$ ) to accommodate two wedges.

The two channels require readout windows of different size. The fringe tracking channel is read out fast and requires a sufficiently small window (e.g.,  $16 \times 32$  pixel) on the detector. The image motion tracking window, on the other hand, requires a larger read-out window ( $32 \times 32$  or  $64 \times 64$  pixel) because of the defocused beams and the beam walk. An update of the FFTS detector readout electronics<sup>5</sup> is under way and first modes are available (Beckmann et al. private communication). The initial orientation of the detector head has been changed. The filter wheel has been rotated by  $90^\circ$  around the optical axis. With periscope and wedges adding to the total height of the detector head, in the new orientation the detector head fits nicely in between science filter wheel and dichroic (Fig. 5).

#### 4. SUMMARY & OUTLOOK

We have presented an update of the opto-mechanical design of the LINC-NIRVANA fringe and flexure tracker system, separating fringe and flexure (image motion) channels on the FFTS detector. A periscope solution with extrafocal defocus (25mm) and demagnification (factor 3), as well as the inclusion of wedges for compensation of atmospheric differential refraction (at  $40^\circ$  and  $60^\circ$  zenith distance) is foreseen.

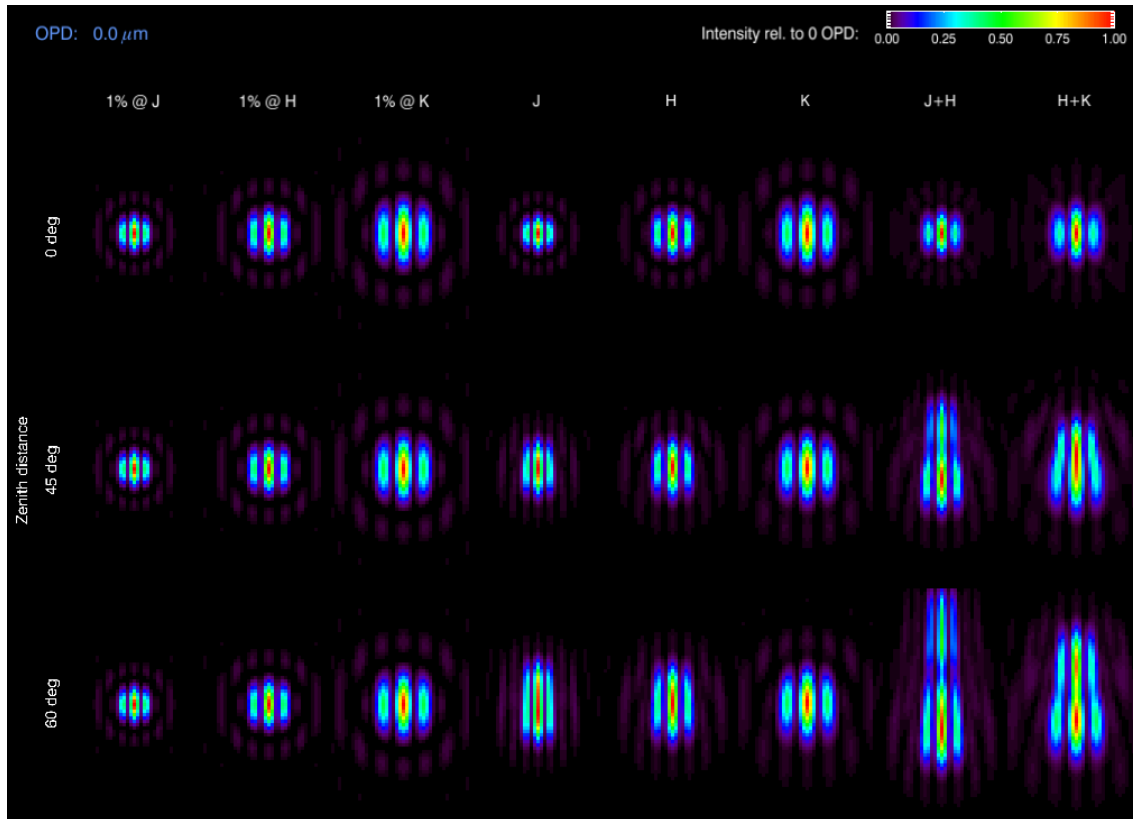


Figure 6. Effects of atmospheric differential refraction. Shown are zero OPD PSFs for all FFTS bandpasses as a function of zenith distance. Obviously, the  $J$ ,  $J + H$ , and  $H + K$  bands are changing significantly (perpendicular to the baseline) with zenith distance.

Next steps focus on the finalization and then realization of the opto-mechanical design, building the detector head housing and the cooling connections. Furthermore functional and performance tests for the new optical components will be developed.

## 5. ACKNOWLEDGMENTS

This work is supported by BMBF 05A08PKA.

## REFERENCES

- [1] Herbst, T., Ragazzoni, R., Andersen, D., Boehnhardt, H., Bizenberger, P., Eckart, A., Gaessler, W., Rix, H., Rohloff, R., Salinari, P., Soci, R., Straubmeier, C., and Xu, W., “LINC-NIRVANA: a Fizeau beam combiner for the large binocular telescope,” in [*Interferometry for Optical Astronomy II*], W. A. Traub, ed., *Proc. SPIE* **4838**, 456–465 (Feb. 2003).
- [2] Straubmeier, C., Eckart, A., Bertram, T., Zealouk, L., and Wang, Y., “The correction of piston aberrations at the LBT: A near-infrared Fringe and Flexure Tracker for LINC,” in [*Interferometry for Optical Astronomy II*], W. A. Traub, ed., *Proc. SPIE* **4838**, 1271–1281 (Feb. 2003).
- [3] Horrobin, M., Eckart, A., Lindhorst, B., Lindhorst, U., Moser, L., Rost, S., Straubmeier, C., Tremou, E., Wank, I., and Zuther, J., “Fringe detection and piston variability in LINC-NIRVANA,” in [*Optical and Infrared Interferometry II*], *Proc. SPIE* **7734** (2010).
- [4] Rost, S., Eckart, A., Horrobin, M., Lindhorst, B., Lindhorst, U., Moser, L., Straubmeier, C., Tremou, E., Wank, I., Zuther, J., and Bertram, T., “The LINC-NIRVANA fringe and flexure tracker: control design overview,” in [*Optical and Infrared Interferometry II*], *Proc. SPIE* **7734** (2010).

- [5] Beckmann, U., Behrend, J., Bohnhardt, H., Connot, C., Driebe, T. M., Heininger, M., Herbst, T. M., Hofmann, K.-H., Nussbaum, E., Schertl, D., Solscheid, W., Straubmeier, C., and Weigelt, G. P., “The fringe and flexure tracking detector of the lbt linc-nirvana beam-combiner instrument,” *New Frontiers in Stellar Interferometry* **5491**(1), 1445–1453, SPIE (2004).
- [6] Bertram, T., Eckart, A., Lindhorst, B., Rost, S., Straubmeier, C., Tremou, E., Wang, Y., Wank, I., Witzel, G., Beckmann, U., Brix, M., Egner, S., and Herbst, T., “The linc-nirvana fringe and flexure tracking system,” *Optical and Infrared Interferometry* **7013**(1), 701327, SPIE (2008).
- [7] Farinato, J., Ragazzoni, R., Arcidiacono, C., Giorgia, G., Diolaiti, E., Foppiani, I., Lombini, M., Schreiber, L., Lorenzetti, D., D’Alessio, F., Causi, G. L., Pedichini, F., Vitali, F., Herbst, T., Kürster, M., Bizenberger, P., Briegel, F., Bonis, F. D., Egner, S., Gässler, W., Mohr, L., Pavlov, A., Rohloff, R. R., and Soci, R., “The mcao wavefront sensing system of linc-nirvana: status report,” *Advances in Adaptive Optics II* **6272**(1), 627229, SPIE (2006).
- [8] Tremou, E., Eckart, A., Horrobin, M., Lindhorst, B., Lindhorst, U., Moser, L., Rost, S., Smajic, S., Straubmeier, C., Wank, I., Zuther, J., and Bertram, T., “The LINC-NIRVANA fringe and flexure tracker: laboratory tests,” in [*Optical and Infrared Interferometry II*], *Proc. SPIE* **7734** (2010).
- [9] Straubmeier, C., Bertram, T., Eckart, A., Rost, S., Wang, Y., Herbst, T., Ragazzoni, R., and Weigelt, G., “The imaging fringe and flexure tracker of linc-nirvana: basic opto-mechanical design and principle of operation,” *Advances in Stellar Interferometry* **6268**(1), 62681I, SPIE (2006).
- [10] Green, R. M., [*Spherical astronomy*], Cambridge University Press (1985).
- [11] Eckart, A., Witzel, G., Kunneriath, D., König, S., Straubmeier, C., Bertram, T., Zamaninasab, M., Schödel, R., Muzic, K., Tremou, E., Meyer, L., Rost, S., Vogel, S., Wiesemeyer, H., Sjouwerman, L., and Herbst, T., “Prospects for observing the galactic center: combining lbt linc-nirvana observations in the near-infrared with observations in the mm/sub-mm wavelength domain,” *Optical and Infrared Interferometry* **7013**(1), 70134L, SPIE (2008).